Scientia Iranica, Vol. 11, Nos. 1&2, pp 69–80

SCIENTIA
IRANICA

Simulation of Mould Filling in the EPC Process

S.M.H. Mirbagheri*, R. Babai[1], M. Dadashzadeh[2], M.T. Ahmadian[3] and P. Davami[1]

In this investigation for Expandable Pattern Casting (EPC) simulation, an algorithm was developed to calculate the gas pressure of the evaporated foam during mould filling. Also, the effect of backpressure evaporative foam on filling behavior was modeled with a new experimental function by adding a Volume Of Fraction (VOF) function. The simulation of molten flow and track free surfaces is based on the (SOLution Algorithm) SOLA-VOF numerical technique. To simulate the three-dimensional incompressible flow of melt in EPC moulds, the pressure boundary conditions, heat transfer and foam gas pressure effect were modified. In order to verify the computational results of simulation melt flow in EPC casting, a thin grey iron plate was poured into a transparent foam mould. Mould filling and foam depolymerization were recorded with a 16mm high-speed camera. The comparison of experimental and simulation results of the sequence filling of EPC casting showed a good consistency, which confirms the accuracy of the model.

INTRODUCTION

Recently, several investigations have been carried out to simulate the filling of thin-walled EPC and full mould castings by coupling heat transfer, fluid flow and the decomposition kinetics of polystyrene [1,2]. Results have demonstrated that when metal is poured, the polystyrene pattern begins to decompose immediately and a violent gas evolution is developed. This causes an increase in pressure at the metal/foam interface and affects liquid metal flow during mould filling, which has a decisive influence on the final casting quality. The behavior of gas pressure, due to the decomposing EPS pattern during mould filling, is very important for designing an appropriate gating system and eliminating defects such as cold shut or impurity and gas entrapment. Also, it will influence the temperature distribution of liquid metal, the solidification sequence and, particularly, the melt permeability [3].

The fluid flow phenomenon during the filling of EPC is, basically, a transient flow problem with the metal/foam interface. The foam removal is governed by the rate of heat exchange between the metal and foam, which, in turn, is defined by a heat transfer coefficient and gaseous foam pressure in the gap between the metal and solid foam. It is very difficult to measure the metal/foam heat transfer coefficient directly, particularly with high melting point metals. However, the foam removal rate can be easily estimated by measuring the speed of the metal/foam interface [2].

In earlier studies, two Computational Fluid Dynamics (CFD) techniques, namely, Marker And Cell (MAC) and SOLA-VOF, had been found to be suitable for fluid flow problems of this kind [3-5]. Since then, different models have been developed, based on the Simplified Marker And Cell (SMAC) [4] technique, Smoothed Particle Hydrodynamics (SPH) [6], SOLA-MAC technique [7], Quasi 3-D-VOF and the Finite Element Method (FEM) [8,9].

The MAGMA Corporation and the RMRC Institute developed their own versions of the 3-D models, based on 3-D-VOF and their particular analytical algorithms, for solving the flow field by the Finite Difference Method (FDM) [10-14]. The Flow Science Institute developed a finite difference code, called FLOW3-D, to simulate the mould filling phenomena [15]. Davami and Mirbagheri modified the Advance Solution Algorithm (ASOLA-VOF) technique for EPC, via global interpolation between new and old time steps, using a shape function only for the EPC process [14]. They developed a CFD code for simulation of the filling

*. *Corresponding Author, Department of Materials Science and Engineering, Sharif University of Technology, P.O. Box 11365-466, Tehran, I.R. Iran.*
1. *Department of Materials Science and Engineering, Sharif University of Technology, Tehran, I.R. Iran.*
2. *Razi Metallurgical Research Center, Tehran, I.R. Iran.*
3. *Department of Mechanical Engineering, Sharif University of Technology, Tehran, I.R. Iran.*

sequence of casting called SUTCAST [11,14]. Lipinsky reviewed the advantages and disadvantages of various methods of solving CFD codes, which can be useful for researchers and engineers [13]. In spite of published literature, more studies are still needed on the effect of backpressure on the filling stage in the EPC process, because, due to a very complex mechanism of foam depolymerization, its modeling still remains a challenge.

In this study, the SOLA-VOF technique has been modified to account for the backpressure effect during the EPC process. The proposed model is capable of considering the effect of various parameters, such as the rate of burning foam, volume of gap, gap gas pressure and the permeability and thickness of refractory coating, as well as foam density. The model was then tested on the EPC benchmark for cast iron.

THE GOVERNING EQUATIONS

In the simulation of mould filling in the EPC casting process, the fluid flow phenomena are governed by mass, momentum and energy conservation equations. These can be described as follows [16]:

a) The momentum transport equation is given by:

$$\frac{D\vec{V}}{Dt} = -\frac{\nabla P}{\rho} + \vec{g} + \frac{\mu}{\rho}\nabla^2\vec{V}, \tag{1}$$

where $\vec{V} = u\hat{i} + \nu\hat{j} + w\hat{k}$ is the velocity vector, P the pressure, $\vec{g}$ the body acceleration vector, ρ the density, μ the viscosity and t is the time;

b) The continuity equation for the liquid-solid region given by:

$$\frac{\rho_L - \rho_S}{\rho}\left[\frac{\partial f_L}{\partial t} + (\vec{\nu}).\nabla f_L\right] + \nabla.(\vec{\nu}) = 0, \tag{2}$$

where $f_s\rho_s + f_l\rho_l = \rho$ and $f_S + f_L = 1.f_S, f_L$ are solid and liquid fractions, respectively;

c) The heat transfer equation for the liquid or solid zone (single phase) is:

$$\rho C_P\frac{\partial T}{\partial t} = -\rho C_P\vec{\nu}.\nabla T + \nabla.\vec{q}. \tag{3}$$

d) The heat transfer equation for the mushy region (two phases) is:

$$\rho\Delta H_f\frac{\partial f_L}{\partial t} = -\rho\Delta H_f\vec{v}.\nabla f_L - \nabla\vec{q}, \tag{4}$$

$$q_x = -k\frac{\partial T}{\partial x}, \quad q_y = -k\frac{\partial T}{\partial y}, \quad q_z = -k\frac{\partial T}{\partial Z}, \tag{5}$$

where $\vec{q} = q_x\hat{i} + q_y\hat{j} + q_z\hat{k}$ is the heat flux. The most commonly used method to describe free surfaces is the VOF method. The VOF method enables tracking of the transition free surface with arbitrary topology and deformation. In the VOF technique, a function $F(x, y, z, t)$ is defined, which is the fractional volume of control element occupied by fluid. F can vary from zero to unity; the cell, having F values between zero and one $(0 < F < 1)$, represents the free surface. $F = 0$ indicates that the cell contains no fluid and $F = 1$ corresponds to a cell filled with fluid. The position of the interface, curvature and normal direction to the free surface can all be determined from the derivatives of F values in a control volume. Because F is a discontinuous function, its derivatives must be controlled in a special way [14-16].

e) The time dependence of F is described by the following equation:

$$\frac{\partial F}{\partial t} + \nabla.\vec{\nu}F = 0. \tag{6}$$

f) The decomposition function of foam (polystyrene) for high melting point metals is:

$$P_s = P_0 + aP_\circ V_g^2 T(V_c - \Delta V_F)^{-2}T_\circ^{-1}$$

$$\text{if} \quad T \leq 1500^\circ\text{ C},$$

$$P_{co} = nRT(kS^n)^{-1},$$

$$\Delta V_{\text{Foam}} = \sum P_{er}^b e^m (F_{i,j,k}^{n+1} - F_{i,j,k}^n)$$

$$\text{if} \quad \varepsilon_F \leq F \leq 1 - \varepsilon_F. \tag{7}$$

In this new model, P_s is the gas pressure of foam decomposition entering the mould cavity during casting, P_0 the initial pressure, V_c the volume of mould cavity, P_{er} the hot permeability, e the coating thickness, S the coating area over the free surface and $a, b, k, m, n (a = 1.5, b = 1.20, \varepsilon_F = 10^{-3}, k = 0.77$ and $n = 0.9 - 1.1)$ are constant parameters [14,17].

SOLUTION METHOD

Finite Difference Approximations

Since the purpose of the current study is the modeling of backpressure, due to the burning of foam on mould filling, only finite difference approximations of the free surface function and setting of the boundary conditions at the free surface are mentioned; the rest appear in the Appendix.

Finite difference approximation of free surface

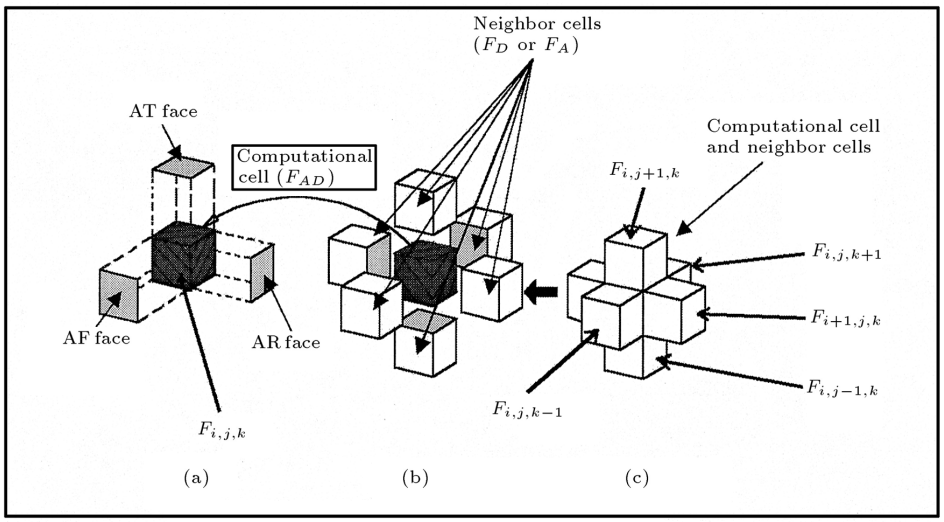

Figure 1. Definition of quantities used in the free-surface boundary condition (Equation 8); a) Discretization faces for computational cell; b) Discretization neighbor cells; c) Assemble cells.

function is [18-20]:

$$F_{i,j,k}^{n+1} - F_{i,j,k}^{n} = -\frac{\overline{\delta t}}{VC_{i,j,k}}$$

$$\left\{\frac{1}{\Delta x}\left[AR_{i+1,j,k}U_{i+1,j,k}^{n+1}F_{i+1,j,k} - AR_{i-1,j,k}U_{i-1,j,k}^{n+1}F_{i-1,j,k}\right]\right.$$

$$+\frac{1}{\Delta y}\left[AT_{i,j+1,k}V_{i,j+1,k}^{n+1}F_{i,j+1,k} - AT_{i,j-1,k}V_{ij-1,k}^{n+1}F_{i,j-1,k}\right]$$

$$\left.+\frac{1}{\Delta Z}\left[AF_{i,j,k+1}W_{i,j,k+1}^{n+1}F_{i,j,k+1} - AF_{i,j,k-1}W_{i,j,k-1}^{n+1}F_{i,j,k-1}\right]\right\}$$

$$\overline{\delta t} = (\delta t^{n} + \delta t^{n+1})/2, \tag{8}$$

where, AR, AT and AF are fractions of the right, top and front face, respectively and VC is cell volume open to flow, which has been shown in Figure 1. Balance for free surface is satisfied by setting the surface cell pressure, P_{cell}, equal to the value obtained by a linear interpolation between foam gas pressure at the surface, P_S, and pressure inside the fluid, P_N [8].

$$D_{i,j,k} = \delta P = (1-\eta)P_N + \eta P_S - P_{\text{cell}},$$

$$\eta = \frac{d_c}{d} = \frac{d_c}{d_c - d_s} = \left(1 - \frac{d_s}{d_c}\right)^{-1},$$

$$d_s = \begin{cases} d_w(0.5 - F_{i,j,k}) & \text{if } F_{i.j,k} > 0.5\ S \\ d_w 0.5(1 + S - \sqrt{8SF_{i.j,k}} & \text{if } F_{i,j,k} \le 0.5\ S \end{cases}$$

$$S = \left|\frac{\text{slope}}{\text{scale}}\right|,$$

$$d_w = \begin{cases} \Delta x & \text{if } UNV \text{ of surface} = i \\ \Delta y & \text{if } UNV \text{ of surface} = j \end{cases}. \tag{9}$$

As shown in Figure 2, d_c is the distance between the cell centers, d_w is the width of the cell of the surface and d_s is the distance from the centre of the surface cell to the fluid surface, UNV is unit normal vector of the surface and S is the surface ratio. Details of slope and scale are referred to in [14].

Donor-Acceptor Flux Approximations

The donor-acceptor method is a convection algorithm. The essential idea is to use information of the F function, downstream as well as upstream of a flux boundary, in order to establish an approximate interface shape. This shape is then used to compute the flux. The VOF method differs somewhat from its predecessors in two respects. First, it uses information about the slope of the surface to improve the flux algorithm. Second, the F function is used to define

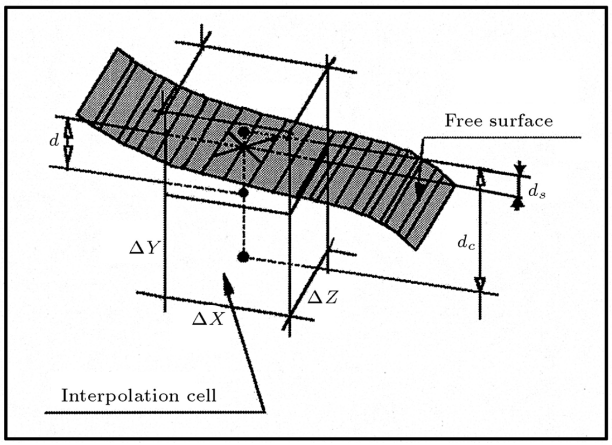

Figure 2. Interpolations free surface in three-dimensional space.

a surface location and orientation for the application of different boundary conditions, which include surface tension forces [19,20].

The free surface cell, (i,j,k), is defined as a cell containing a non-zero value of F and having at least one neighboring cell, $(i \pm 1, j, k), (i, j \pm 1, k)$ and $(i, j, k \pm 1)$, that contains a zero value of F. In a surface cell, it is assumed that the free surface can have only one orientation (mainly horizontal or vertical in each $x-y, x-z$ and $z-y$ planes), in which the liquid is mainly located adjacent to only one of the six sides of the cell. Some surface orientations result in cells with nonzero values of F and empty neighbor cells $((i \pm 1, j, k), (i, j \pm 1, k)$ and $(i, j, k \pm 1))$. These are treated as full cells [19]. The free surface orientation can be tracked with a cell flag array, $NF(i,j,k)$, as shown in Table 1.

Convection Algorithm

At each face of the 3-D computing cell, the two neighboring cells immediately adjacent to the interface are distinguished, one becoming a donor cell and the other an acceptor cell and cell quantities are given the subscripts D and A, respectively, e.g., F_D and F_A. One 3-D cell has six faces and six neighboring cells where each adjacent cell has the label F_D or F_A and six faces will have label F_{AD}. As shown in Figure 3, the labeling is accomplished by means of the algebraic sign of the fluid velocity normal to the interface; the donor cell is always upstream and the acceptor cell downstream, with respect to the interface. It is emphasized that the D and A labels are assigned, separately, for each face of a cell. Thus, each cell will have six separate assignments of D or A, corresponding to its faces. The face value of F, denoted by F_{AD}, which appears in Equation 8, will be either F_D or F_A, chosen according to the algorithm in Figure 3. The final value of the face F is denoted by F'_{AD}. It is the final F'_{AD} which, when convected with the fluid velocity normal to the interface, will not remove more fluid per unit area, nor more void per unit area, than the donor cell contains, even when the face is completely open to flow [8,18]. Below is the redefinition of F'_{AD}, assuming that F_{AD} has already been determined at the right (R^+), front (F^+), top (T^+), left (R^-), back (F^-) and bottom (T^-) faces of the cell, for this case [11,14,19]:

$$\delta F_x^{R+} = F_{AD} U_{i+1,j,k}^{n+1} \delta t = \text{sgn}\left[U_{i+1,j,k}^{n+1}\right] \min \left[F_{AD}\left|\forall_x^{R+}\right| + CFXR^+, \quad F_D \Delta X_D\right], \quad \text{(10a)}$$

$$\delta F_y^{F+} = F_{AD} V_{i,j+1,k}^{n+1} \delta t = sgn\left[V_{i,j+1,k}^{n+1}\right] \min \left[F_{AD}\left|\forall_y^{F+}\right| + CFYF^+, \quad F_D \Delta y_D\right], \quad \text{(10b)}$$

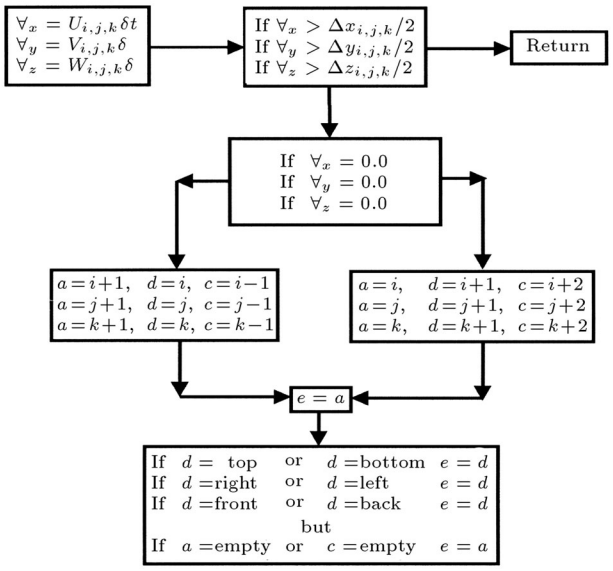

Figure 3. The employed algorithm to determine the donor-acceptor cell.

Table 1. Definition of NF array values.

Flag Number	Cell Type	Neighbor Cell Conditions	Free Surface Orientation
$NF = 0$	Fluid cell	No void cells adjacent	Does not bisect
$NF = 8$	Void cell	No fluid in cell	
$NF = 1$	Surface cell	Neighbor fluid cell to the left	Mainly parallel to Y direction
$NF = 2$	Surface cell	Neighbor Fluid cell to the right	
$NF = 3$	Surface cell	Neighbor fluid cell to the bottom	Mainly parallel to X direction
$NF = 4$	Surface cell	Neighbor fluid cell to the top	
$NF = 5$	Surface cell	Neighbor fluid cell to the back	Mainly parallel to Z direction
$NF = 6$	Surface cell	Neighbor fluid cell to the front	
$NF = 7$	Isolated cell	All adjustment cells are void	Indeterminate orientation

$$\delta F_z^{T+} = F_{AD} W_{i,j,k+1}^{n+1} \delta t = sgn\left[W_{i,j,k+1}^{n+1}\right] \min \left[F_{AD}\left|\forall_z^{T+}\right| + CFZT^+, \quad F_D \Delta z_D\right], \tag{10c}$$

$$\delta F_x^{R-} = F_{AD} U_{i-1,j,k}^{n+1} \delta t = sgn\left[U_{i-1,j,k}^{n+1}\right] \min \left[F_{AD}\left|\forall_x^{R-}\right| + CFXR^-, \; F_D \Delta X_D\right], \tag{10d}$$

$$\delta F_y^{F-} = F_{AD} V_{i,j+1,k}^{n+1} \delta t = sgn\left[V_{i,j+1,k}^{n+1}\right] \min \left[F_{AD}\left|\forall_y^{F-}\right| + CFYF^-, \quad F_D \Delta y_D\right], \tag{10e}$$

$$\delta F_z^{T-} = F_{AD} W_{i,j,k-1}^{n+1} \delta t = sgn\left[W_{i,j,k-1}^{n+1}\right] \min \left[F_{AD}\left|\forall_z^{T-}\right| + CFZT^-, \quad F_D \Delta z_D\right], \tag{10f}$$

where:

$$\forall_x^{R+} = U_{i+1,j,k}^{n+1}\delta t, \quad \forall_y^{F+} = V_{i,j+1,k}^{n+1}\delta t,$$

$$\forall_z^{T+} = W_{i,j,k+1}^{n+1}\delta t, \quad \forall_x^{R-} = U_{i-1,j,k}^{n+1}\delta t,$$

$$\forall_y^{F-} = V_{i,j-1,k}^{n+1}\delta t, \quad \forall_z^{T-} = W_{i,j,k-1}^{n+1}\delta t,$$

$$CFXR^+ = \max\Big[(1.0 - F_{AD})\left|\forall_x^{R+}\right| - (1.0 - F_D)\,\Delta X_D, \quad 0.0\Big], \tag{10g}$$

$$CFYF^+ = \max\Big[(1.0 - F_{AD})\left|\forall_y^{F+}\right| - (1.0 - F_D)\,\Delta y_D, \quad 0.0\Big], \tag{10h}$$

$$CFZT^+ = \max\Big[(1.0 - F_{AD})\left|\forall_z^{T+}\right| - (1.0 - F_D)\,\Delta z_D, \quad 0.0\Big], \tag{10i}$$

$$CFXR^- = \max\Big[(1.0 - F_{AD})\left|\forall_x^{R-}\right| - (1.0 - F_D)\,\Delta X_D, \quad 0.0\Big], \tag{10j}$$

$$CFYF^- = \max\Big[(1.0 - F_{AD})\left|\forall_y^{F-}\right| - (1.0 - F_D)\,\Delta y_D, \quad 0.0\Big], \tag{10k}$$

$$CFZT^- = \max\Big[(1.0 - F_{AD})\left|\forall_z^{T-}\right| - (1.0 - F_D)\,\Delta z_D, \quad 0.0\Big]. \tag{10l}$$

The min term, used in Equations 10a to 10f prevents a flux of more fluid per unit area than the donor cell and the max term of Equations 10g to 10l prevents a flux of more voids per unit area than the donor cells contain.

Interface Orientation Within a Surface Cell

Following the calculation of the new F-values, the code sweeps the mesh, redefining the new cell types and assigning the appropriate flags, $NF_{i,j,k}$. At the same time, the approximate direction of the fluid in each surface cell is determined and a pressure interpolation neighbor cell is assigned. Determination of whether the fluid is mostly horizontal or vertical in a surface cell relies on estimating the local slope of the fluid/void interface. It is assumed that the interface is a straight-plane segment partitioning the cell. As shown in Figure 4, the slope of the free surface is estimated by introducing six of the surface-height functions $L(x_j) - L(x_k), L(y_i) - L(y_k), L(z_i) - L(z_j)$ in a 3-D space. A good approximation of LF derivatives (gradient of F) is [11]:

$$\begin{cases} \dfrac{\partial LF_{xy}}{\partial y}_j = \dfrac{\left[(L(x)_{j+1} - L(x)_j)\frac{\Delta y_T}{\Delta y_B} + (L(x)_j - L(x)_{j-1})\frac{\Delta y_B}{\Delta y_T}\right]}{\Delta y_T + \Delta y_B} \\ \dfrac{\partial LF_{xz}}{\partial z}_k = \dfrac{\left[(L(x)_{k-1} - L(x)_k)\frac{\Delta z_{\text{front}}}{\Delta z_{\text{back}}} + (L(x)_k - L(x)_{k-1})\frac{\Delta z_{\text{back}}}{\Delta z_{\text{front}}}\right]}{\Delta z_{\text{front}} + \Delta z_{\text{back}}} \end{cases} \tag{11a}$$

$$\begin{cases} \dfrac{\partial LF_{yx}}{\partial x}_i = \dfrac{\left[(L(y)_{i+1} - L(y)_i)\frac{\Delta x_r}{\Delta x_l} + (L(y)_i - L(y)_{i-1})\frac{\Delta x_l}{\Delta x_r}\right]}{\Delta x_l + \Delta x_r} \\ \dfrac{\partial LF_{yz}}{\partial z}_k = \dfrac{\left[(L(y)_{k-1} - L(y)_k)\frac{\Delta z_{\text{front}}}{\Delta z_{\text{back}}} + (L(y)_k - L(y)_{k-1})\frac{\Delta z_{\text{back}}}{\Delta z_{\text{front}}}\right]}{\Delta z_{\text{front}} + \Delta z_{\text{back}}} \end{cases} \tag{11b}$$

$$\begin{cases} \dfrac{\partial LF_{zx}}{\partial x}_i = \dfrac{\left[(L(z)_{i+1} - L(z)_i)\frac{\Delta x_r}{\Delta x_l} + (L(z)_i - L(z)_{i-1})\frac{\Delta x_l}{\Delta x_r}\right]}{\Delta x_l + \Delta x_r} \\ \dfrac{\partial LF_{zy}}{\partial y}_j = \dfrac{\left[(L(z)_{j-1} - L(z)_j)\frac{\Delta y_t}{\Delta y_b} + (L(z)_j - L(z)_{j-1})\frac{\Delta y_b}{\Delta y_t}\right]}{\Delta y_t + \Delta y_b} \end{cases} \tag{11c}$$

$$L(x)_j = L(x)_k = F_{i-1,j,k}\Delta x_{i-1} + F_{i,j,k}\Delta x_i + F_{i,+1j,k}\Delta x_{i+1},$$

$$L(y)_k = L(y)_i = F_{i,j-1,k}\Delta y_{j-1} + F_{i,j,k}\Delta y_j + F_{i,j+1,k}\Delta y_{j+1},$$

$$L(z)_j = L(y)_i = F_{i,j,k-1}\Delta z_{k-1} + F_{i,j,k}\Delta z_k + F_{i,j,k+1}\Delta z_{k+1}.$$

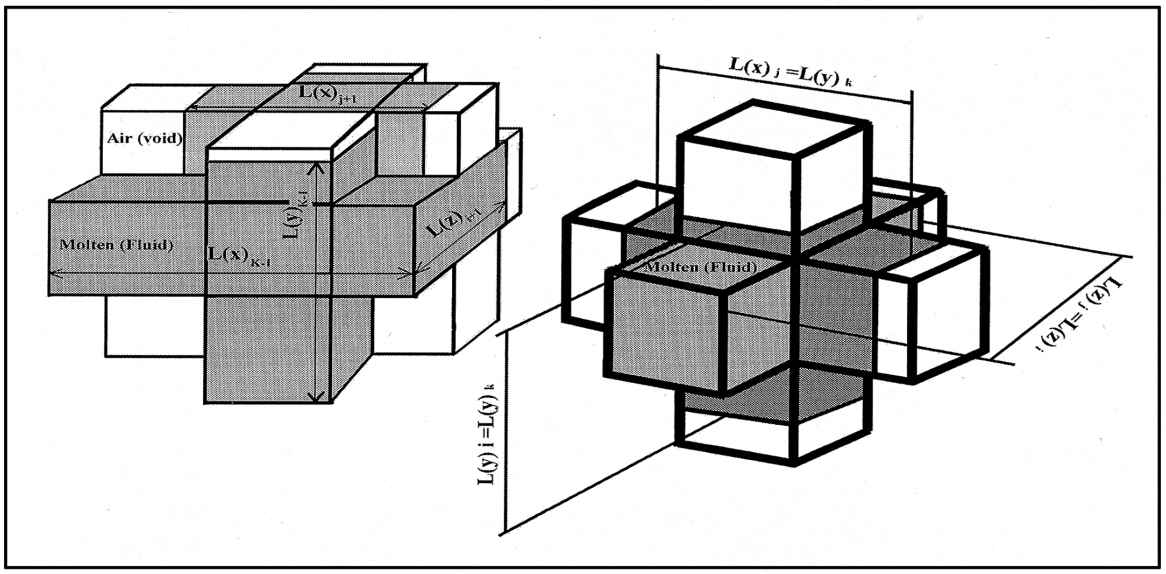

Figure 4. The surface-high functions for calculating slope of free surface.

This procedure will produce simple derivatives of surface-height function in the invariable mesh, especially for cubic cells with equal dimensions (i.e., $\Delta z = \Delta x = \Delta y$). Once the boundary slope and the side occupied by fluid have been determined, a plane can be constructed in the cell with the correct amount of volume lying on the F fluid side. This plane is used as an approximation to the actual boundary and provides the information to calculate η for application of free surface pressure boundary conditions.

ALGORITHEM

i) Semi-explicit approximation of Equations A4 to A6 are used to compute the first guess for new, time-level velocities, using the initial conditions or previous time-level values for all advective, pressure and viscous accelerations;

ii) To satisfy the continuity equation, Equation A7, pressures are iteratively adjusted in each cell and the velocity changes induced by each pressure change (δP) are added to the velocities computed in Step i. The pressure change (δP) for full cell, surface cell and interior void cell is calculated from [8,19]:

$$\delta P_{i,j,k} = D_{i,j,k}\left[\frac{\delta t}{\rho}\left(\frac{1}{\Delta x}\left(\frac{1}{\Delta x_l}+\frac{1}{\Delta x_r}\right)+\frac{1}{\Delta y}\left(\frac{1}{\Delta y_t}+\frac{1}{\Delta y_b}\right)+\frac{1}{\Delta y}\left(\frac{1}{\Delta z_{\text{front}}}+\frac{1}{\Delta z_{\text{back}}}\right)\right)\right]^{-1}$$

for full cell, (12)

$$\delta P_{i,j,k} = (1-\eta)P_N + \eta P_S - P_{i,j,k}$$

for surface cell. (13)

In this model, cells that are partially full and surrounded by fluid are classed as void interior cells. The pressure in such a cell is calculated by a weighted average approach:

$$\delta P_{i,j,k} = \sum_{m=1}^{6} wP_m \Big/ \sum_{m=1}^{6} w_m - P_{i,j,k}$$

for interior void cell. (14)

where, P_N is the interpolated pressure in neighbor cells and P_S is the foam gas pressure acting on the free surface given by Equation 7. For an interior cell, $w = 1$, if the neighboring cell contains fluid and $w = 0$, if it does not. An iterative scheme should be applied because of the change in cell pressure during each time step;

iii) The F function defining fluid regions must be updated to give the new fluid configuration;

iiii) Finally, the temperature in each cell is calculated by means of Equation A1 and, then, the solid or liquid fraction of metal in each cell is determined.

Repetition of the above steps will advance a solution through any desired time interval. At each step, of course, a suitable boundary condition must be imposed at all meshes and free surface boundaries.

RELAXATION FACTORS

In some cases, the over-relaxation factor, ω, is used to accelerate the convergence of the iteration by mul-

tiplying δP from Equation 12 by ω. An optimum value of ω is often between 1.7 and 1.8, but it should not exceed 2.0, otherwise, in Equation 15, an unstable iteration condition will result [19].

$$\delta P_{i,j,k} = D_{i,j,k}\beta_{i,j,k},$$

$$\beta_{i,j,k} = \omega\left[\frac{\delta t}{\rho}\left(\frac{1}{\Delta x}\left(\frac{1}{\Delta x_l}+\frac{1}{\Delta x_r}\right)+\frac{1}{\Delta y}\left(\frac{1}{\Delta y_t}+\frac{1}{\Delta y_b}\right)+\frac{1}{\Delta y}\left(\frac{1}{\Delta z_{\text{front}}}+\frac{1}{\Delta z_{\text{back}}}\right)\right)\right]^{-1}. \quad (15)$$

However, a problem arises with the surface cell. These cells are strongly dependent on adjacent fluid cells and, therefore, the use of an under-relaxation factor is required. This should prevent the solution from diverging. The under-relaxation factor accommodates the dependency between the surface cell and the interpolation cell. It is applied to the interpolation cell and slows down the changes that may occur in pressure and velocity during the pressure iteration. Since the interpolation of the surface pressure is a function of η, it is natural that the under-relaxation factor should, itself, be a function of this value. Table 2 shows, under-relaxation factors [8]. In this table, l, m, n are matrix indices of the interpolation cell; i, j, k are matrix indices for a surface cell; ΔW is the width of the cell tangential to the surface; Ω is an implicit factor and β is the partial derivative of $D_{i,j,k}$. However, in this investigation, a new under-relaxation factor has been developed, based on the idea behind the original SOLA-VOF model [8,14]:

$$\omega'_{i,j,k} = \left[1 - \frac{\beta_{\text{Int}_{l,m,n}}(1-\eta_{i,j,k})}{\beta_{s_{i,j,k}}}\right]. \quad (16)$$

The interpolation β_{Int} and surface β_S are calculated from Equation 15. However, for calculating β_S, d is employed as the surface cell dimension, dependent on the free surface UNV. For example, in Figure 2, for calculating β_S, the values of $\Delta y_s = d$, $\Delta x_S = \Delta x_{Int}$ and $\Delta z_S = \Delta z_{Int}$ are substituted in Equation 15, because the UNV of the free surface is the vector **j**.

RESULT AND DISCUSSION

Experimental Results

To understand the fluid dynamics of mould filling in the EPC process, a flask was built that allowed for direct observation of mould filling through a Pyrex window. The flask, shown in Figure 5, was designed to fit into a larger vibratory flask to allow for sand

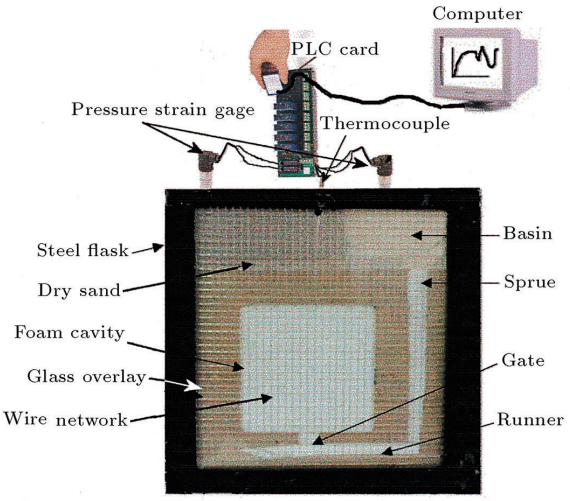

Figure 5. Flask with one-transparency face for technique photography.

Table 2. Vertical plate gravity casting-simulation data.

Material: Cast Iron [wt]	C = 3.8, Si = 2.2, Mn = 0.75, S < 0.1, P < 0.2,
Pouring Temperature [°C]	1350 ± 5
Thermal Conductivity [cal/sec cm°C]	$k_L = 0.069, K_s = 0.07, k_{\text{sand}} = 0.001$
Heat of Fusion [cal/gr]	$\Delta H_f = 49.76$
Viscosity [cm^3/sec]	$\mu = 0.02368$
Specific Heat [cal/gr °C]	$C_P^l = 0.23, C_p^S = 0.21, C_p^{\text{sand}} = 0.23$
Density [gr/cm^3]	$\rho_L = 7.2, \rho_S = 7.3, \rho_{\text{sand}} = 1.61, \rho_{\text{Foam}} = 0.014$
Transformation Temperature [°C]	$T_L = 1270 \pm 1, T_S = 1150 \pm 1$
Number Elements of Cavity	N=8022045
Dimension Elements of Cavity [cm]	$\Delta x = \Delta y = \Delta z = 0.20$
CPU Time for Pentium III 600 [min]	20
Boundary Conditions	Wall: Free slip
	Intel: Gage pressure = 15_{mbar}

compaction. The pattern used in the experiments was made using an EPC bead with a grade C (sieve size 36-60, AFS 38 gfn, raw size 0.508-0.254 mm and density = 0.014 g/cm^3) [17]. After the foam pattern and gating systems are assembled, using an adhesive (a glue joint type), they are, then, dipped (except for one of the faces of foam plat) in a refractory slurry or coating, removed and rotated slowly to insure the coating covers all foam surfaces and allowed to dry. The coating is a thixotropic liquid mixture of refractory particles (including silica, alumina, mica, alumina-silicates and mullite), dispersants, thixtropic agents and binders in a water carrier. The silica sand used was AFS 50 gfn. Gluing the foam pattern to a sheet of Pyrex, coating the pattern and placing that assembly in the flask assembled the apparatus. The flask was vibrated while it was filled with sand. Finally, molten metal was poured and the mould filling was recorded with a 16-mm high-speed camera, capable of taking 285 frames/sec. The pressure of the foam pyrolysis product was recorded by a data acquisition system. The geometry, dimensions and gating system ratios are shown in Figure 6 for a vertical benchmark plate with cross-section with a foam pattern. Experiments were run using cast grey iron. The gating system is non-pressurized with the gating ratio 1.0:1.1:2.0 (down sprue: runner: ingate). The photograph, using a high-speed camera, of the filling of the EPC mould with grey iron in Figure 7, showed that metal filled the mould as quickly as the pattern degraded. A large gas gap was observed between the liquid metal and foam pattern during filling. Figure 8 shows that the pressure in the cavity obtained from the data acquisition system (after filtering), abruptly decreases from 4840 Pa to 22 Pa at point M of curve P-t; after 3641 milliseconds. In this case, mould filling was controlled by the pattern degradation and was at

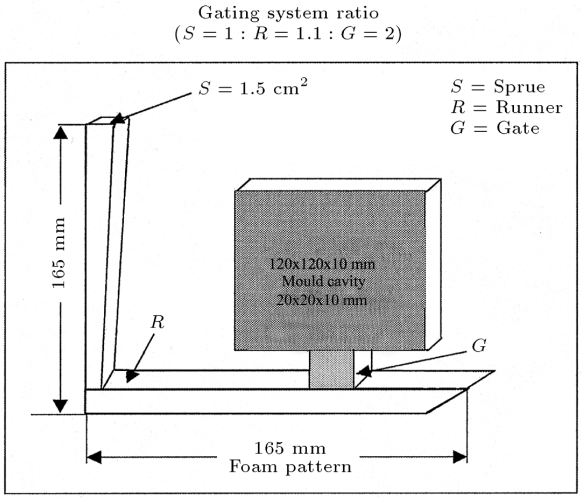

Figure 6. Schematics of geometry and dimensions of benchmark plate.

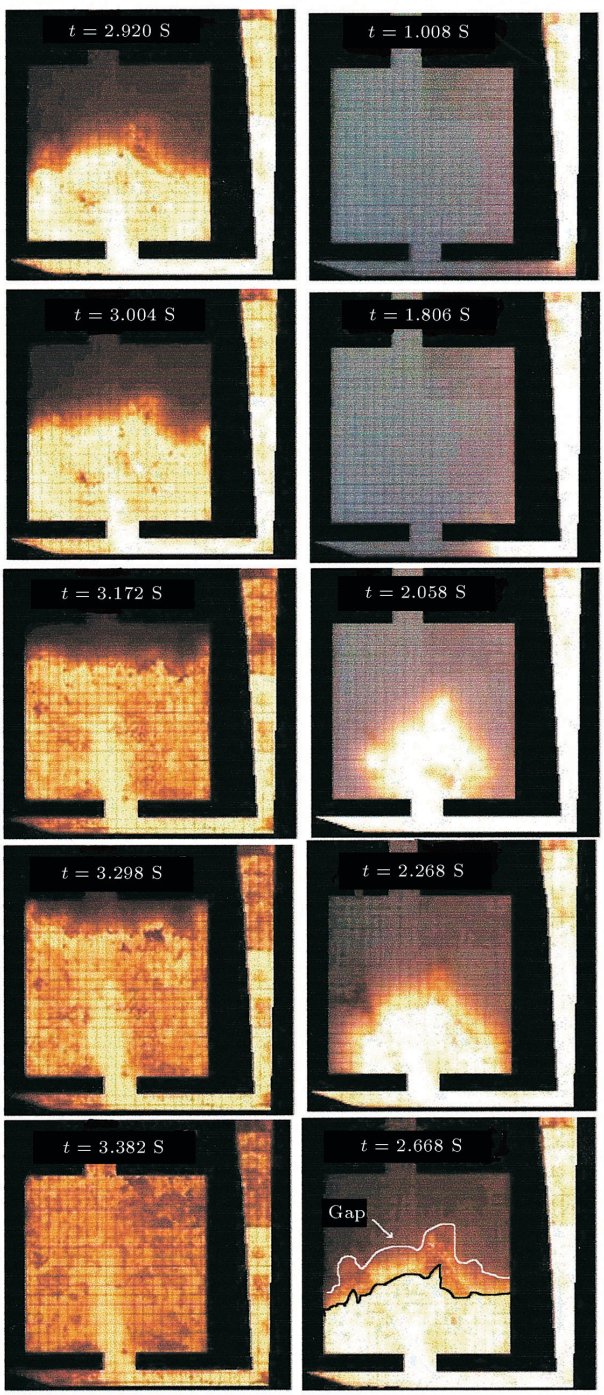

Figure 7. Photography results for EPC process; molten: Gray iron; mould: Unbounded silica sand.

an approximate velocity of 60-65mm/sec (total filling time of cavity was 3.38 sec.). Gas, evolved to the burning foam (by molten metal with a temperature over 1300°C), flowed through the sand very quickly and escaped from the flask at the edges of the Pyrex window during mould filling. The fact that these gases ignited during mould filling indicated that they were volatile gases, not the inert products that would be expected upon complete depolymerization of the

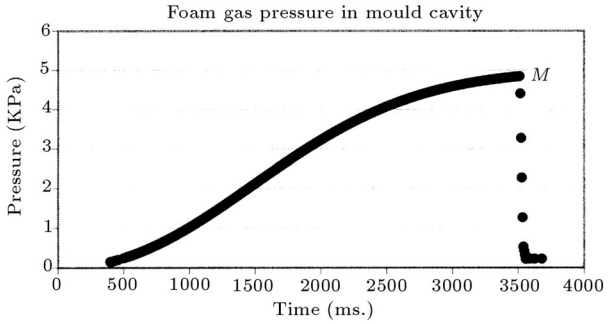

Figure 8. Changing of pressure during mould filling stage in EPC process.

foam pattern. Figure 9 shows simulated results, using data in Table 3. The predicted flow pattern, filling sequences and temperature distribution are the same as the observed results shown in Figure 7.

Discussion

The comparison between experimental results obtained via the use of a high-speed camera (Figure 7) and simulated results (Figure 9), verify that the predicted flow patterns are correct. Also, a mathematical model (Equation 9) was developed to calculate the effect of backpressure, due to evaporative foam, on the filling behavior, which showed a good consistency and which confirms the accuracy of the new model. Regarding the high-speed photographic camera study of the mould filling during the EPC process, it is observed that the foam elimination takes place by different mechanisms for casting high melting point ($T_m > 1000°C$) and low melting point alloys. For example, when aluminum alloys ($T_m < 720°C$) are cast, the foam melts and very little depolymerization (foam evaporate) occurs in the mould cavity [21,22]. When grey iron ($T_m > 1300°C$) is cast, much more depolymerization occurs and a lot of gas is produced. In the EPC process, the dominant mould filling mechanism is due to the backpressure

Table 3. Modes of under-relaxation functions [9].

	Modes	Under-Relaxation Function
1	None	$\omega'_{i,j,k} = 1.0$
2	Linear	$\omega'_{i,j,k} = (1-(1-\eta_{i,j,k})\beta_{l,m,n})^{-1}$
3	Original SOLA-VOF	$\omega'_{i,j,k} = \left[1-\beta_{l,m,n}\frac{(1-\eta_{i,j,k})\Delta t}{d_c\Delta\omega}\right]^{-1}$
4	Modified SOLA-VOF	$\omega'_{i,j,k} = \left[1-\beta_{l,m,n}\frac{(1-\eta_{i,j,k}\Delta t}{\rho d_c\Delta\omega}\right]^{-1}$
5	Wang's correction	$\omega'_{i,j,k} = \left[1-\omega_0\frac{(1-\eta_{i,j,k}\Delta t}{4\Omega}\right]^{-1}$
6	Wang's empirical	$\omega'_{i,j,k} = (2.428-(1-\eta_{i,j,k})1.285)^{-1}$

for high melting point alloys, while, for low melting point alloys, surface tension controls the mould filling process [21]. The present CFD code can predict flow pattern, filling sequence and temperature distribution in the molten grey cast iron, throughout the filling and solidification period of the EPC casting.

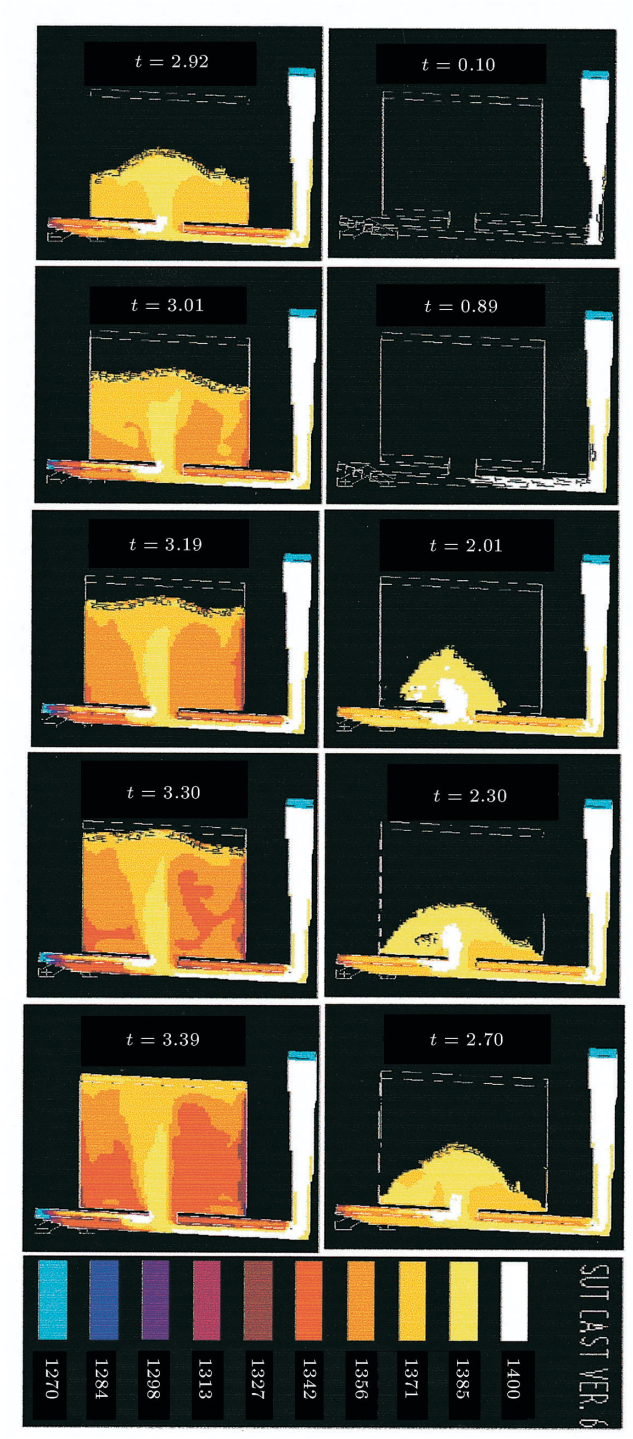

Figure 9. Simulation results of mould filling in the EPC process; molten: Gray iron; mould: Unbounded silica sand.

CONCLUSIONS

The computational fluid dynamics code (SUTCAST) developed in this work can simulate the combined effects of heat transfer, depolymerization of the foam and fluid flow during the filling of metal casting. It can predict the flow pattern, burn rate of foam, filling sequence and temperature distribution in the metal and the mould throughout the filling and solidification period of the EPC casting with a complex shape. Experimental results show that in the EPC process, the dominant mould filling mechanism is backpressure for high melting point alloys. Also, the filling time in the foam moulds is a little more than sand moulds. This difference of time is due to backpressure resulting from:

i) Foam decomposition,

ii) Heat expansion of gas cavity,

iii) Heat expansion of refractory coating and the closeness of coating porosity,

iiii) Compression of cavity foam gas during the filling stage.

The results of simulation show good agreement with the experimental results. This code can be used to analyze a casting design by computer and provides very useful information for casting design, including fluid flow pattern and filling sequence, possibility of premature freezing, shrinkage zone, solidification map and hot zone. Therefore, this package is a powerful and flexible tool for analyzing a casting design to help reduce cost and the time consuming process of designing complex casting moulds.

ACKNOWLEDGMENTS

This work was supported by the Razi Metallurgical Research Centre (RMRC) under Grant No, SUT.CST-110-1982. Also, the authors gratefully acknowledge the assistance of the Department of Materials, Imperial College, London, UK.

REFERENCES

1. Tseng, C.H. "A study of the mould filling parameters in the evaporative pattern casting process", Ph.D. Thesis, Missouri-roll University, USA (1991).
2. Lee, H.S. "Gating of full mould castings with unbounded sand mould", *AFS Cast Metals Research Journal*, **9**, pp 112-116 (1973).
3. Harlow, J.E., Shannon, P.J. and Welch, J.E. "The MAC method: A computing technique for solving viscous, incompressible transient fluid flow problems involving free surface", *Technical Report LA-3425*, Los Alamos National Laboratory, Los Alamos, New Mexico 87545 (1968).
4. Amsden, A.A. and Harlow, H.F. "The SMAC method: A numerical technique for calculating incompressible fluid flow", *Technical Report LA-4337*, Los Alamos National Laboratory, Los Alamos, New Mexico 87545 (1970).
5. Hirt, C.W., Nichols, B.D. and Romero, N.C. "SOLA-A numerical solution algorithm for transient fluid flows", *Technical Report LA5852*, Los Alamos National Laboratory, Los Alamos, New Mexico 87544 (1975).
6. Ha, J., Cleary, P. and Nguyen, T. "Simulation of die filling in gravity casting using SPH method", *Second International Conference on CFD in the Minerals and Process Industries CSIRO*, Melbourne, Australia, pp 423 (1999).
7. Lewis, R.W., Ravindran, L. and Tran, D.V. "Finite element simulation of the benchmark mould filling problem", *Modelling of Casting, Welding and Advanced Solidification Processes VII Proceeding* (1995).
8. Elliot, S.D. "Fluid flows aspects of solidification modeling: Simulation of low-pressure die-casting", Ph.D. Thesis, Queensland University, Australia (1999).
9. Lin, H.J. and Hwang, W.S. "Three-dimensional fluid flow simulation for mould filling", *AFS Transaction*, pp 855-862, (1989).
10. Lipinski, M., Schaefer, W. and Andersen, S. "Modelling of combined heat and fluid flow for deformation of filling sequence of real complex shaped casting", *Modelling Control of Casting and Welding Processes V Proceeding*, pp 771-776 (1990).
11. Davami, P. and Mirbagheri, S.M.H. "Solidification simulation of parts casting", Available at http:// www.sutcast.com.
12. Razavi, H. and Davami, P. "Solidification simulation of gravity casting of Al-12%-Si in permanent mould with computer simulation of heat transfer in air gap", *59th. World Foundry Congress*, CIATF (1992).
13. Lipinski, M.D. "Mould filling simulation for casting processes", Ph.D Thesis, Rheinisch-Westfalischen Technischen Hochschule Aachen, Germany (English) (1996).
14. Mirbagheri, S.H.M., Davami, P. and Varahram, N. "3-D computer simulation melts flow in lost foam casting process", *Int. Journal for Num. Methods in Engineering*, **58**, pp 723-748 (2003).
15. Nichols, B.D. and Hirt, C.W., *Lost Foam Casting Simulation*, Flow Science, Inc., Available at http:// www.flow3d.com.
16. Wang, C.W. "Computer modeling of fluid flow and heat transfer in metal casting", Ph.D. Thesis, Pittsburgh University, USA (1990).
17. Monroe, R.M., *Expendable Patterns Casting*, American foundryman's Society Inc., pp 84-100 (1992).
18. Torrey, M.D., Cloutman, L.D. and Hirt, C.W. "NASA-VOF2D: A computer program for incompressible flows with free surfaces", *Technical Report LA10642-MS*, Los Alamos National Laboratory, Los Alamos, New Mexico 87545 (1985).

19. Torrey, D.M., Mjolsness, R.C. and Stein, L.R. "NASA-VOF3-D: A three-dimensional computer program for incompressible flow with free surface", *Technical Report LA11009-MS*, Los Alamos National Laboratory, Los Alamos, New Mexico 87545 (1987).

20. Hirt, C.W. and Nichols, B.D. "Volume of fluid method for the dynamics of free boundary", *Journal of Computational Physics*, **39**, pp 201-225 (1981).

21. Tseng, H. and Askeland, D. "Study of EPC mould filling process using metal velocity and mass energy balances", *AFS Transaction* 1992, **98**, pp 519-527 (1992).

22. Sun, Y., Askeland, D. and Tsai, H. "Investigation of wetting and wicking properties of refractory coating in the EPC process", *AFS Transaction*, **98**, pp 297-308 (1992).

APPENDIX

Finite Difference Approximation

a) The finite difference approximation of the heat transfer equation is:

$$T_{i,j,k}^{n+1} = T_{i,j,k}^{n} - \Delta t\Big[(UTX + VTY + WTZ) + (DQX + DQY + DQZ)\Big],$$

$$UTX = 0.5\Big\{(1+\alpha)U_{i-1,j,k}(DTXL) + (1-\alpha)U_{i,j,k}(DTXR)\Big\},$$

$$DTXL = \frac{T_{i,j,k} - T_{i-1,j,k}}{\Delta x},$$

$$DTXR = \frac{T_{i+1,j,k} - T_{i,j,k}}{\Delta x},$$

$$DQX = \frac{QXR - QXL}{\rho C_P \Delta x},$$

$$QXR = -k_R \frac{T_{i+1,j,k}^{n} - T_{i,j,k}^{n}}{\Delta x},$$

$$QXL = -k_l \frac{T_{i,j,k}^{n} - T_{i-1,j,k}^{n}}{\Delta x}. \quad \text{(A1)}$$

In the freezing range, the specific heat and liquid fraction of the mushy metal is found through the following equation:

$$C_p^{LS} = \frac{\Delta H_f - \alpha \Delta H_{\text{Foam}}}{T_l - T_s}, \quad T_s \langle T \langle T_l, \quad \text{(A2)}$$

$$F_{L_{i,j,k}} = \frac{T_{i,j,k} - T_s}{T_l - T_s}, \quad T_s \le T \le T_l, \quad \text{(A3)}$$

where T_S, T_L are solidus and liquidus temperature, respectively [14]. Discussion for calculation of heat convection terms VTY and WTZ and heat diffusion terms DQY and DQZ are quoted in [19]:

b) The finite difference approximation of the momentum transport equation is:

$$U_{i,j,k}^{n+1} = U_{i,j,k}^{n} + \Delta t\Big[\frac{P_{i,j,k}^{n+1} - P_{i+1,j,k}^{n+1}}{\rho \Delta x} + g_x - FUX - FUY - FUZ + VISX\Big], \quad \text{(A4)}$$

$$V_{i,j,k}^{n+1} = V_{i,j,k}^{n} + \Delta t\Big[\frac{P_{i,j,k}^{n+1} - P_{i,j+1,k}^{n+1}}{\rho \Delta y} + g_Y - FVX - FVY - FVZ + VISY\Big], \quad \text{(A5)}$$

$$W_{i,j,k}^{n+1} = W_{i,j,k}^{n} + \Delta t\Big[\frac{P_{i,j,k}^{n+1} - P_{i,j,k+1}^{n+1}}{\rho \Delta z} + g_Z - FWX - FWY - FWZ + VISZ\Big], \quad \text{(A6)}$$

$$FUX = \frac{U_{i,j,k}^{n}}{2\Delta x}\Big[DUL + DUR + \alpha \text{Sign}(U_\alpha)(DUL - DUR)\Big],$$

$$DUL = U_{i,j,k}^{n} - U_{i-1,j,k}^{n},$$

$$DUR = U_{i+1,j,k}^{n} - U_{i,j,k}^{n},$$

$$U_\alpha = (DUR + DUL)/2,$$

$$VISX = v\Big(\frac{U_{i+1,j,k}^{n} - 2U_{i,j,k}^{n} + U_{i-1,j,k}^{n}}{\Delta x^2} + \frac{U_{i,j+1,k}^{n} - 2U_{i,j,k}^{n} + U_{i,j-1,k}^{n}}{\Delta y^2} + \frac{U_{i,j,k+1}^{n} - 2U_{i,j,k}^{n} + U_{i,j,k-1}}{\Delta z^2}\Big),$$

where the superscript (n) stands for old time level and $(n+l)$ for the new time level. However, discussion for the calculation of advective flux terms; *FUY, FUZ, FVX, FVY, FVZ, FWX, FWY, FWZ* and the viscous flux terms; *VISY, VISZ*, are quoted in [18-20].

c) The finite difference approximation to the continuity equation is:

$$D_{i,j,k} = \Big(\frac{U^{n+1}_{i,j,k} AR_{i,j,k} - U^{n+1}_{i-1,j,k} AR_{i-1,j,k}}{\Delta x} + \frac{V^{n+1}_{i,j,k} AT_{i,j,k} - V^{n+1}_{i,j-1,k} AT_{i,j-1,k}}{\Delta y} + \frac{W^{n+1}_{i,j,k} AF_{i,j,k} - W^{n+1}_{i,j,k-1} AF_{i,j,k-1}}{\Delta z} + M_{i,j,k} \Big) / AC_{i+1/2,j+1/2,k+1/2=0}$$

$$\begin{cases} M_{i,j,k} = \frac{\rho_L - \rho_S}{\rho} \left(DFT + UFX + VFY + WFZ \right), \\ \quad \text{if } 0 \langle f_{L_{i,j,k}} \langle 1 \\ M_{i,j,k} = 0 \\ \quad \text{Otherwise,} \end{cases}$$

$$AR_{i-1,j,k} = \theta_{i-1,j,k}, \quad AT_{i,j-1,k} = \theta_{i,j-1,k},$$

$$AF_{i,j,k-1} = \theta_{i,j,k-1},$$

$$AC_{i+1/2,j+1/2,k+1/2} = \theta_{i+1/2,j+1/2,k+1/2},$$

$$DFT = \frac{f^{n+1}_{L_{i,j,k}} - f^{n}_{L_{i,j,k}}}{\Delta t},$$

$$\frac{f^{n}_{L_{i+1,j,k}} - f^{n}_{L_{i-1,j,k}}}{2\Delta x} UFX = 0.5 \left(U_{i,j,k} + U_{i-1,j,k} \right),$$

$$\frac{f^{n}_{L_{i,j+1,k}} - f_{L_{i,j-1,k}}}{2\Delta y} VFY = 0.5 \left(V_{i,j,k} + V_{i,j-1,k} \right),$$

$$WFZ = 0.5 \left(W_{i,j,k} + W_{i,j,k-1} \right) \frac{f^{n}_{L_{i,j,k+1}} - f^{n}_{L_{i,j,k-1}}}{2\Delta z}. \quad \text{(A7)}$$

In Equation A7, AR, AT and AF are the fractions of right, top and front face, respectively and VC is cell volume open to flow, which has been shown in Figure 1. The partial-cell treatments use a step function, $\theta_{i,j,k}$, with values of 0 and 1 in the obstacle material and moving fluid, respectively [19].